The effect of tension compression asymmetry on modelling the bending response of sheet moulding compound composites

Jonathan Tham, Trevor Sabiston, Anna Trauth, Julie Lévesque, Kay A. Weidenmann, Kaan Inal

Angaben zur Veröffentlichung / Publication details:

Tham, Jonathan, Trevor Sabiston, Anna Trauth, Julie Lévesque, Kay A. Weidenmann, and Kaan Inal. 2018. "The effect of tension compression asymmetry on modelling the bending response of sheet moulding compound composites." *Composites Part B: Engineering* 154: 157–65. https://doi.org/10.1016/j.compositesb.2018.07.058.

The effect of tension compression asymmetry on modelling the bending response of sheet moulding compound composites

Jonathan Tham[a], Trevor Sabiston[a], Anna Trauth[b], Julie Lévesque[c], Kay André Weidenmann[b], Kaan Inal[a,*]

[a] Department of Mechanical and Mechatronics Engineering, University of Waterloo, 200 University Avenue West, Waterloo, Ontario, N2L 3G1, Canada
[b] Institut für Angewandte Materialien - Werkstoffkunde, Karlsruhe Institut für Technologie, Engelbert-Arnold-Straße 4, D-76131, Karlsruhe, Germany
[c] Department of Mechanical Engineering, Laval University, Québec, Québec, G1V 0A6, Canada

A B S T R A C T

Phenomenological models are required to predict the behaviour of a glass fibre reinforced Sheet Moulding Compound (SMC) composite material for use in the automotive industry. Material testing is conducted in tension, compression, in-plane shear, and three-point bending. The SMC composite exhibits tension-compression asymmetry and in-plane anisotropy. A model, which incorporates an anisotropic and asymmetric yield function, is developed. The model is calibrated to the experimental tension, compression and in-plane shear tests and are validated using the three-point flexure test. The model captures the flexure response within 8.1% of the experimental observations. The importance of including tension compression asymmetry within the model is demonstrated.

1. Introduction

Fuel economy and safety regulations in the automotive industry are become stricter [1], vehicle manufacturers need to reduce weight and improve crashworthiness. A reduction of vehicle mass by 10% results in a 6.8% fuel economy improvement [2,3]. Sources of weight reduction and improved crashworthiness include material selection, and component design optimization [4]. Depending on the type of reinforcement and matrix material, composites have a higher strength and stiffness to weight ratio than metals [5,6]. In the past, composites were mostly used in low production volume vehicles as composite components were manufactured through low volume production methods, such as hand lay-ups, which were slow and expensive [7]. Interest in composite materials for mass production vehicle components has increasing significantly. High volume manufacturing methods, such as compression moulding, decrease the material and manufacturing costs associated with composites and makes materials such as Sheet Moulding Compounds (SMC), viable for mass-production vehicles [8,9]. Exterior body panels and structural elements of a vehicle can be made of SMC and effect both passenger and pedestrian safety. The Head Injury Criterion (HIC) is a measure of the acceleration experienced by the centre of gravity of the head during an impact, it evaluates the chance of injury or death in an impact between a vehicle body panel and a pedestrians head [10]. The HIC is affected by the stiffness of the body panel, and it is crucial to accurately predict the bending behaviour of SMC composites to evaluate the HIC [10–12].

Vehicle manufacturers use Finite Element Analysis (FEA) to reduce the development cost and time, as designs can be verified in simulations before it is produced and physically tested. In order to use FEA for modeling the structural behaviour of SMC composite components accurately, a material model which is capable of capturing the fundamental behaviour of the SMC is required. The model not only has to be accurate, but also fast, in order to reduce the development time of composite components [13].

Due to the inclusion of fibres into the matrix material for reinforcement, the resulting material behaviour is more complex than each of the constituent phases on their own. Micromechanics based multi-scale approaches are commonly used to model the homogenized response of these materials [14,15]. Sabiston et al. have developed a unit cell model, with a functionally graded interphase zone to model the elasto-visco-plastic behaviour of long fibre composites [16,17]. Carmen et al. applies an micromechanics approach to short-fibre composites to predict the composite stiffness and local stress variations [18]. The advantage of using a micromechanics model is its ability to determine local stresses and strains, which is useful in modelling fracture in the material. However, material properties of the individual

* Corresponding author.
E-mail address: kinal@uwaterloo.ca (K. Inal).

phases, and a method to capture the orientation effects are required. In addition, the interaction between the phases need to be modelled. As a result, using such a model is computationally intensive compared to macro-scale phenomenological models [19,20]. For the model to be effective in simulating composites at a component level, the model needs to be computationally inexpensive.

Macro-scale phenomenological models allow the material to be modelled as a single phase to reduce the computation time associated with multiphase material models. Commercially available composite models built into major finite element software were developed for high volume fraction idealized unidirectional and laminated composites [21]. These commercially available material models in LS-DYNA have been used by Huang et al. [22] and Xiao et al. [23] to model crushing of laminated composite structures. SMC composites exhibit complex behaviour, such as in plane material anisotropy and tension-compression asymmetry, due to the fibre distribution and orientation [9,24,25]. They exhibit an elasto-plastic response due to the fibre orientation and relatively low volume fraction which results in a more dominant matrix material behaviour [26].

Tension-compression asymmetry of polymers is observed from the testing of polymer materials. Donato et al. compares various pressure sensitive yield criterion and their accuracy in capturing the tension-compression asymmetry [27]. The conically modified and parabolically modified von Mises yield criterion compared have a linear and quadratic dependence on the hydrostatic stress respectively [27].

SMC composites exhibit anisotropy due to the moulding process. The flow of material during the manufacturing of the charge and during the moulding process, results in fibre alignment in certain directions leading to anisotropy in the final product [28,29]. Feld et al. [24] studied the degree of process-induced anisotropy caused by various degrees of mould coverage and found that both the moulding process and SMC charge manufacturing process introduced anisotropy to the material. Oldenbo et al. evaluated the effect of process-induced anisotropy on the global stiffness of a SMC panel, showing that the impact of the moulding process on anisotropy can be reduced by the selection of the initial charge placement [25].

In order to be able to capture the observed behaviour of the SMC composite, an anisotropic yield function which is capable of capturing tension-compression symmetry is required. The yield criterion by developed Cazacu et al. [30] for hexagonal closed packed metals has the functionality to capture the response of SMC. It incorporates a parameter to capture tension-compression asymmetry and uses a linear transformation on the deviatoric stress tensor to capture anisotropy.

In this work, a macroscopic phenomenological anisotropic elasto-plastic model capable of capturing elastic and plastic tension-compression asymmetry is developed to model the non-linear behaviour of the SMC composite. The phenomenological approach uses the observed material behaviour from experiments, in tension, compression and in-plane shear, to calibrate the material model. The model is validated by predicting the flexure response of the SMC composite. The importance of the capturing the tension compression asymmetry within the elastic and plastic response is demonstrated.

2. Material and testing

This section covers the quasi-static experimental testing conducted on glass fibre reinforced polymer SMC plaques. Standardized testing is performed for uniaxial tension, compression, in-plane shear and three-point bending. The tests performed are quasi-static at strain rates $10^{-2}/s$ and below. The calculated average stress-strain curves from the raw experimental results are used to calibrate and validate the material model implemented in this work.

2.1. Material composition and processing

The SMC plaques are composed of a glass fibre reinforced filled polyester matrix. The polyester matrix also contains styrene and filler material such as hollow glass spheres and calcium carbonate. The fibre volume fraction is approximately 18.3%. The SMC plaques were moulded from SMC charges manufactured by adding randomly oriented chopped glass fibres, which have a fibre length of approximately 25 mm, in between two layers of matrix material. The charges were compression moulded and cured at $150°C$ to create the finished plaques.

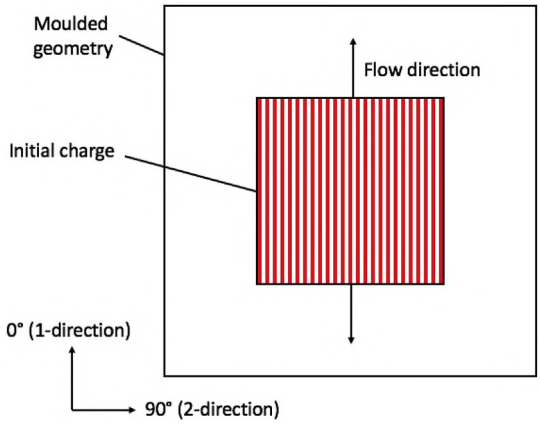

Fig. 1. Illustration of a moulded SMC plaque showing the material directions with respect to the flow direction during moulding.

The tests for tension, compression and bending are conducted in both the 0° and 90° directions, which are aligned with and perpendicular to the flow direction of the material during the moulding process respectively. The plaques for tension and compression are 457 mm square with a 2 layer charge covering 38% of the mould. The plaques for bending and shear are 457 mm by 254 mm with a 3 layer charge covering 25–36% of the mould. The charges have the same aspect ratio as the mould for both instances. The material directions are defined in Fig. 1, the flow direction also aligns with the material rolling direction of the SMC.

2.2. Test specimens

Tensile testing is performed using ASTM D3039 [31]. Tensile testing is completed in the 0° and 90° directions to measure the in-plane anisotropy of the composite under a tensile load. The tensile testing specimens are rectangular specimens with the dimensions given in Table 1. The specimens are clamped in a tensile testing fixture with one end fixed, while the other end is loaded at 2 mm/min in the tensile direction. The strain is measured using digital image correlation (DIC).

The compressive testing is performed according to ASTM D6641 [32] in the 0° and 90° directions. The test is carried out in a combined loading compression test, where both an end and shear load is applied to the specimen in order transfer load to the specimen effectively without damaging the gripped areas. The compressive test specimens are rectangular specimens with the dimensions given in Table 1. The gripped faces are reinforced by aluminum tabs, attached using an epoxy-based adhesive, to eliminate failure within the gripping fixture. The axial strains are measured on both sides of the specimen using strain gauges. The strains on each side are compared to verify that the specimen did not buckling during testing using the percent bending threshold of 10% as per ASTM D6641 [32]. The specimens are loaded at 1 mm/min in the compressive direction.

In-plane shear testing is performed according to ASTM D5379 [33]. In this test, forces are applied to the specimen in opposing directions through a loading fixture to generate an area of maximum shear stress at the centre of the specimen [34]. The specimens used are rectangular specimens with 90° V-notches at the centreline [33]. The dimensions of the specimens are given in Table 1. DIC is used to obtain the in-plane shear strain of the specimen. The specimens are loaded at 1.5 mm/min.

Table 1
Test specimen dimensions [31–33,35].

Tensile		Compressive		Shear		Bending	
Parameter	Value (mm)	Parameter	Value (mm)	Parameter	Value (mm)	Parameter	Value (mm)
Overall length	250	Overall length	140	Overall Length	76	Overall Length	80
Width	25	Width	12	Overall width	19	Width, b	10
Grip length	37.5	Untabbed length	13	Gauge length	2.5	Support length, L	58
Thickness	2.4	Thickness	2.4	Thickness	3.4	Thickness, d	2.8
		Strain gauge length	2	Gauge section width	11.21	Loading fixture radius	5
				Notch radius	1.3	Support fixture radius	2

The three-point bend or flexure testing, in the 0° and 90° directions of the moulded SMC plaque, is performed according to DIN EN ISO 178 [35]. In this test, a rectangular specimen is supported at two locations, while a load is applied by a loading fixture at the centre of the specimen in the through thickness direction [35]. The specimen and fixture dimensions are given in Table 1. The specimens are loaded at 1 mm/min in the vertical direction.

The flexure strain and stress is calculated with equations (1) and (2) respectively [35]. The variables D and P are the deflection at the centre of the specimen and the load applied by the loading fixture respectively.

$$\varepsilon_{flexure} = \frac{6Dd}{L^2} \tag{1}$$

$$\sigma_{flexure} = \frac{3PL}{2bd^2} \tag{2}$$

2.3. Experimental results

The average experimental stress-strain curves for the tensile and compressive tests in the 0° and 90° directions, and the in-plane shear test are plotted on the same axes in Fig. 2a to determine the behaviour of the SMC composite in various loading directions. From the comparison of the tension and compression results, it is evident that tension-compression asymmetry in present in both the 0° and 90° directions, where the material is stiffer in compression than tension for both loading directions. In addition, in-plane anisotropy is also observed between the 0° and 90° directions, the material is stiffer in the 0° direction in both tension and compression. As suggested by literature, the anisotropy is caused by the slight orientation of the fibres induced by the manufacturing process of the composite [28,29]. Both the elastic and plastic regime are anisotropic and asymmetric in tension and compression. The tensile tests also fail at a significantly lower strain compared to the compressive tests, this is due to a difference in failure mode in tension and compression. In-plane anisotropy is also observed in the flexure experiments, this is shown in Fig. 2b which compares the average flexure stress-strain curves in the 0° and 90° directions. Error bars are also plotted in Fig. 2b to show the variation in the experimental results. Overall, the material behaviour of this SMC composite, which includes the stiffer response in compression than tension and the presence of in-plane anisotropy, is similar to the behaviour observed in literature.

3. Material model development

A non-linear elasto-plastic material model for explicit dynamic analysis is implemented in order to capture the complex behaviour of the SMC composite observed in experimental results. A forward Euler integration scheme is used in the SMC material model.

3.1. Elastic model

In order, to capture the in-plane anisotropy due to the orientation of the chopped glass fibres, the orthotropic elastic stiffness tensor ($\mathbb{L}_{el}$) is required. It is calculated using equations (3) and (4), where E are the elastic moduli, G are the shear moduli and ν are the Poisson's ratios [36]. It is orthotropic with respect to the 0° and 90° directions. The 0° direction, 90° direction and through-thickness direction are aligned with the 1, 2 and 3-directions respectively.

$$\mathbb{L}_{el} = \begin{bmatrix} \frac{1-\nu_{23}\nu_{32}}{E_2E_3\Delta} & \frac{\nu_{21}+\nu_{31}\nu_{23}}{E_2E_3\Delta} & \frac{\nu_{31}+\nu_{21}\nu_{32}}{E_2E_3\Delta} & 0 & 0 & 0 \\ \frac{\nu_{12}+\nu_{13}\nu_{32}}{E_3E_1\Delta} & \frac{1-\nu_{31}\nu_{13}}{E_3E_1\Delta} & \frac{\nu_{32}+\nu_{31}\nu_{12}}{E_3E_1\Delta} & 0 & 0 & 0 \\ \frac{\nu_{13}+\nu_{12}\nu_{23}}{E_1E_2\Delta} & \frac{\nu_{23}+\nu_{13}\nu_{21}}{E_1E_2\Delta} & \frac{1-\nu_{12}\nu_{21}}{E_1E_2\Delta} & 0 & 0 & 0 \\ 0 & 0 & 0 & 2G_{12} & 0 & 0 \\ 0 & 0 & 0 & 0 & 2G_{23} & 0 \\ 0 & 0 & 0 & 0 & 0 & 2G_{31} \end{bmatrix} \tag{3}$$

$$\Delta = \frac{1-\nu_{12}\nu_{21}-\nu_{23}\nu_{32}-\nu_{31}\nu_{13}-2\nu_{12}\nu_{23}\nu_{31}}{E_1E_2E_3} \tag{4}$$

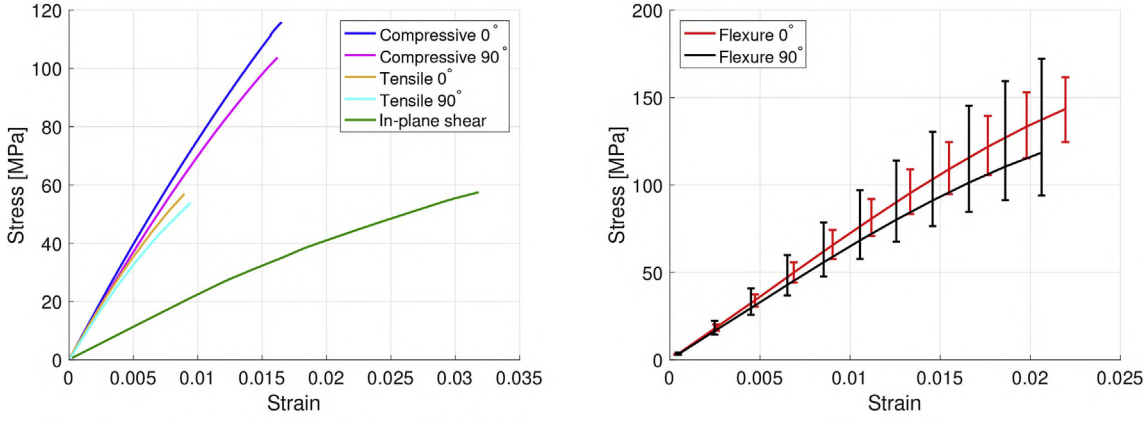

(a) Tension, compression and in-plane shear (b) Flexure

Fig. 2. Average experimental stress-strain response.

In order to capture the tension-compression asymmetry in the elastic behaviour of the composite, the stress triaxiality, T, is used to determine if the material is in tension or compression. Stress triaxiality is calculated using equation (5), where I_1 and J_2 are calculated using equations (6) and (7) respectively. σ is the stress, while $\mathbf{S}$ is the deviatoric stress, calculated using equation (8). A simple criterion is implemented where the material is considered to be in compression if the triaxiality is negative, and tension if it is positive. The components of the elastic stiffness matrix for the normal directions are assigned either the tensile modulus or compressive modulus depending on the triaxiality for the current stress state.

$$T = \frac{I_1}{3\sqrt{3J_2}} \tag{5}$$

$$I_1 = \sigma_{11} + \sigma_{22} + \sigma_{33} \tag{6}$$

$$J_2 = \frac{1}{2}\mathbf{S}\colon \mathbf{S} \tag{7}$$

$$\mathbf{S} = \sigma - \frac{1}{3}I_1 \tag{8}$$

3.2. Yield function

Based on the experimental results, there is an observed tension-compression asymmetry and in-plane anisotropy in yielding. Therefore, a yield criterion capable of capturing this behaviour is required. The orthotropic yield criterion developed by Cazacu et al. [30], shown in equation (9), is selected for this purpose. The orthotropic yield criterion by Cazacu et el. is able to capture the tension-compression asymmetry through the use of the k parameter shown in equation (9) [30]. The degree of asymmetry is controlled through the a exponent and F is the effective stress [30]. This yield criterion captures the in-plane orthotropy through a linear transformation of the deviatoric stress tensor, $\mathbf{S}$, with the transformation tensor, $\mathbb{C}$, to obtain Σ, shown in equation (10) [30]. The transformation tensor is defined in equation (11), the C_{ij} terms, where $i = 1{:}\ 3$ and $j = 1{:}\ 3$, control the orthotropy in normal directions, while C_{ii} where $i = 4{:}\ 6$ control the orthotropy in shear [30]. Σ_i are the principal values of the transformed stress tensor.

$$(|\Sigma_1| - k{\cdot}\Sigma_1)^a + (|\Sigma_2| - k{\cdot}\Sigma_2)^a + (|\Sigma_3| - k{\cdot}\Sigma_3)^a = F^a \tag{9}$$

$$\Sigma = \mathbb{C}\colon \mathbf{S} \tag{10}$$

$$\mathbb{C} = \begin{bmatrix} C_{11} & C_{12} & C_{13} & 0 & 0 & 0 \\ C_{12} & C_{22} & C_{23} & 0 & 0 & 0 \\ C_{13} & C_{23} & C_{33} & 0 & 0 & 0 \\ 0 & 0 & 0 & C_{44} & 0 & 0 \\ 0 & 0 & 0 & 0 & C_{55} & 0 \\ 0 & 0 & 0 & 0 & 0 & C_{66} \end{bmatrix} \tag{11}$$

3.3. Hardening rule

Apart from the yield criterion, a hardening rule is also required to model how the stress evolves as the plastic strain increases by relating the effective plastic strain to the flow stress. A power law hardening rule is used to capture the hardening behaviour of the SMC composite. The version of power law hardening rule used is Ludwik's equation [37] given by Equation (12), where $\bar{\sigma}$ is the flow stress, σ_y is the yield stress, $\bar{\varepsilon}_p$ is the effective plastic strain, K is the strength coefficient and n is the strain hardening exponent.

$$\bar{\sigma} = \sigma_y + K(\bar{\varepsilon}_p)^n \tag{12}$$

3.4. Stress integration algorithm

The material model is implemented as a LS-DYNA user-defined material model based on a forward Euler integration scheme. The stresses and effective plastic strain at each time step of the simulation, for each element, are evaluated based on the algorithm proposed by Williams et al. [38,39]. Based on the boundary conditions, the strain increment is provided as an input by the LS-DYNA solver for each element. The algorithm uses the associative flow rule [40], which states that the plastic strain increment is a scalar multiple of the normal to the yield surface.

By comparing the stress calculated using the yield function with the flow stress curve, the amount of plastic strain during the current time step can be calculated. If the effective stress exceeds the flow stress for the current amount of plastic strain, an iterative loop using the Convex Cutting Plane (CCP) algorithm introduced by Abedrabbo et al. [41] is required to determine the amount of plastic strain resulting from the current strain increment, and enforce the yield criterion. The stress and plastic strain during each iteration of this loop are indicated by the subscript s as σ_s and $\bar{\varepsilon}_s$ respectively. $\Delta d\lambda$ is an update to the effective plastic strain increment. $\partial\phi/\partial\sigma$ is the normal to the yield surface, which is the derivative of the yield criterion, ϕ, with respect to the Cauchy stress, while $\partial\bar{\sigma}/\partial\bar{\varepsilon}$ is the derivative of the flow stress expression with respect to the effective plastic strain. This loop iterates until the absolute difference between the equivalent stress and flow stress is less than or equal to 10^{-8}. A flow chart for the framework of the LS-DYNA user-defined material model is shown in Fig. 3.

4. Numerical simulations

The user-defined material model is used to perform finite element simulations of the tensile, compressive and in-plane shear in order to calibrate the model parameters to the experimental test results. The calibrated user-defined material model is then validated by performing flexure test simulations.

The material model is calibrated using an iterative inverse finite element analysis approach, where the stress-strain response from component level simulations is compared to the experimentally measured data to obtain the material model parameters required to capture the observed material behaviour. This method of calibration most closely reproduces the experimental results as it is able to account for the boundary effects in tests such as the compressive test. However, this comes at the cost greater time required to calibrate the model.

The finite element models discussed in this section use the LS-DYNA element formulation 2, a selectively reduced fully integrated solid element. Eight node hexahedral elements with an aspect ratio of 1 were specified. This aspect ratio is not possible in some locations due to the

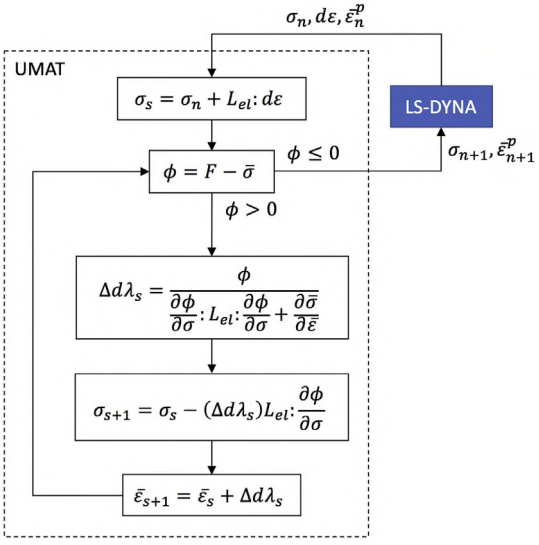

Fig. 3. LS-DYNA user-defined material model framework.

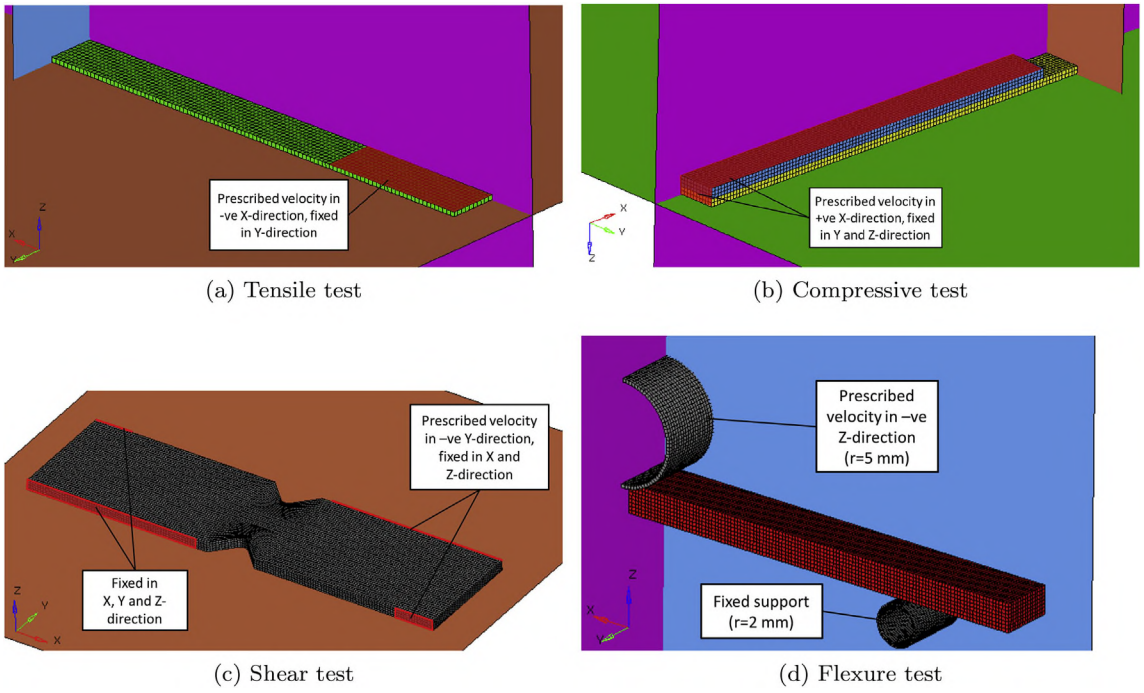

(a) Tensile test (b) Compressive test

(c) Shear test (d) Flexure test

Fig. 4. Finite element models showing symmetry and boundary conditions.

test geometries and local mesh refinement. The finite element mesh for the tensile, compressive, in-plane shear and flexure specimen are shown in Fig. 4.

4.1. Tensile test model setup

The tensile test specimen dimensions are given in Table 1. An eighth symmetry model is used for the tensile test model. There are two elements across the thickness of the specimen. The model is symmetric about the xy-plane, yz-plane and xz-plane. The gripped faces of the specimen are prescribed a tensile velocity in the axial direction and fixed in the transverse direction to reflect the constraints imposed by the stationary and loading grippers of the tensile testing apparatus. The velocity applied is halved, to account for the symmetry boundary conditions, and time scaled by a factor of 1000, to reduce computation time. The finite element mesh, symmetry planes, and boundary conditions applied are shown in Fig. 4a. The mesh consists of 1040 elements, each approximately 1.2 *mm* in size.

4.2. Compressive test model setup

The specimen dimensions for compressive test are given in Table 1. In addition to the SMC specimen, the aluminum tabs were modelled as well, using a linear elastic material model with the properties given in Table 2. The nodes of the aluminum tabs on the surface in contact with the SMC are coincident with nodes along the surface of the SMC representing a perfect bond between the two materials. There are four elements across the thickness of the SMC specimen. Similar to the tensile test model, this model is an eighth symmetry model, symmetric about the xy-plane, yz-plane, and xz-plane. The gripped and end faces of the specimen are prescribed a compressive velocity in the axial direction and fixed in the transverse and through thickness directions. The velocity applied is halved, to account for the symmetry boundary conditions, and time scaled by a factor of 100, to reduce computation time. The displacement is measured by the elongation of the gauge region in the loading direction. The finite element mesh and boundary conditions applied are shown in Fig. 4b. The mesh consists of 5520 elements, approximately 0.5–0.6 *mm* in size.

Table 2
Material properties for aluminum.

Parameter	Value
Elastic Modulus	68.9 *GPa*
Poisson's Ratio	0.33
Density	$2.7 \times 10^{-3} g/mm^3$

4.3. Shear test model setup

The specimen dimensions for the in-plane shear test are given in Table 1. There are twelve elements across the thickness of the in-plane shear specimen model. A half symmetry model about the xy-plane is used for the in-plane shear model. The gripped faces on the stationary end of the specimen are constrained in all translational degrees of freedom. The gripped faces on the loading end is constrained in the translational degrees of freedom along the x and z-direction and prescribed a velocity in the negative y-direction. The model is time scaled by a factor of 1000 to reduce computation time. The finite element mesh and boundary conditions applied are shown in Fig. 4c. The mesh consists of 40320 elements, ranging from approximately 0.1 to 0.5 *mm* in size, with finer elements near the notch radii.

4.4. Flexure test model setup

The specimen dimensions of the flexure test are given in Table 1. Eight elements are used across the thickness of the flexure test specimen. The loading nose and supports were modelled using rigid linear hexahedral elements. A surface to surface contact is defined between the loading nose and the test specimen, and the supports and the test specimen. The coefficient of friction is 0.3 for both contact pairs. The finite element model used is a quarter symmetry model about the xz and yz-planes. The supports were fixed in all translational degrees of freedom, while the loading nose was fixed in the translational degrees of freedom along the x and y-direction and prescribed a velocity in the negative z-direction. The model is time scaled by a factor of 10000 to reduce computation time. The finite element mesh and boundary

Table 3
Elastic and hardening parameters.

Parameter	Value
Tensile Modulus (E_{1T})	7775 *MPa*
Tensile Modulus (E_{2T}, E_{3T})	7150 *MPa*
Compressive Modulus (E_{1C})	8450 *MPa*
Compressive Modulus (E_{2C}, E_{3C})	7950 *MPa*
Shear Modulus (G_{12}, G_{23}, G_{31})	2375 *MPa*
Poisson's Ratio (ν_{12})	0.3
Yield Stress (σ_y)	5 *MPa*
Power Law Hardening Strength (K)	782.89 *MPa*
Power Law Hardening Exponent (n)	0.4226

conditions are shown in Fig. 4d. The mesh consists of 14280 elements, approximately 0.333 *mm* in size.

4.5. Model calibration

Using the finite element models in the LS-DYNA solver, the SMC user-defined material was calibrated against the average of the experimental stress-strain curves of the tensile, compressive and in-plane shear tests in Section 2. Due to the data being limited to in plane properties, it is assumed that $E_3 = E_2$, $G_{23} = G_{31} = G_{12}$, $r_{0C} = r_{0T}$, $r_{90C} = r_{90T}$ and $C_{55} = C_{66} = C_{44}$. The calibrated elastic and hardening parameters, and yield function parameters are summarized in Tables 3 and 4 respectively.

Fig. 5a compares the simulation results to the average experimental results for the tensile, compressive and in-plane shear load cases. The implemented material model is able to successfully replicate the experimentally measured stress-strain behaviour for axial and shear loading. The relative error comparing the simulations to experimental tests for the calibration is shown in Fig. 5b. The Mean Absolute Errors (MAE) [42] for the calibration tests are within 1.5% of the experimental results.

4.6. Flexure test simulation results

Using the calibrated material model the three-point flexure test is simulated using the model detail in Section 4.4. The simulation results for the flexure test are shown in Fig. 6a. The simulation results over predict the average experimental results for the flexure test in both the 0° and 90° directions. However, there is a large variation among the experimental flexure results as shown in Fig. 2b, and the predictions are within this variation. The relative stress-strain response between the both the 0° and 90° directions of the simulations is similar to the experimental results. The relative error for the flexure tests are shown in Fig. 6b. The MAE are 4.8% and 8.1% for the 0° and 90° directions respectively.

5. Discussion

Micromechanics is typically used to model the properties of SMC due to the fibre orientation evolution during the compression moulding process [14,15]. Multiscale modelling is needed to use micro scale data at the part scale, Chen et al. developed a multi-scaling approach for SMC composites and have demonstrated the ability to predict the elastic response of laboratory tests [43]. To model full scale components a phenomenological model is required. The laminate composite fabric material model in LS-DYNA (MAT_058) is the best match to the material behaviour observed in the SMC. It is a composite material model with damage for unidirectional, laminated and fabric composites [21]. The damage model, based on the model developed by Matzenmiller et al. [23,44], and reduces the elastic stiffness as the damage accumulates, which allows for a non-linear stress-strain behaviour to be modelled however it does not account for the plasticity caused by the polymer matrix material. This material model is also only implemented for shell elements.

A phenomenological approach to modelling woven textile composites has been implemented by Ryou et al. to capture the tension compression asymmetry, and anisotropy [45]. Ryou et al. implement tension compression asymmetry in the elastic regime by varying the elastic constants depending on the stress state in a given direction, which violates the elastic relationship of the material system [45]. The selection of the elastic constants on the stress triaxiality for the material ensures that the set of elastic constants is valid. The yield function used herein is more advanced than the Drucker Prager yield function used by Ryou et al. where the anisotropy is captured through the hardening rule [45]. The anisotropy is captured with the yield function in the proposed model.

The predicted flexure response from the simulations shows an over prediction compared to the experimentally measured response. This difference in stress-strain responses could be due to various mechanisms which have not been accounted for. One of these would be the local variation in material properties as the SMC material is not homogeneous. For example, there could be a variation in volume fraction or fibre orientation across the thickness of the specimen. A variation in volume fraction or fibre orientation would result in a variation in material parameters, such as the elastic moduli and hardening coefficients.

A parametric study is conducted in order to study the effects of a through-thickness variation in properties. Although the variation in local material parameters cannot be identified from the macroscopic experimental testing performed, linear distributions are used to quantify the effect of the variation in material properties on the flexure response. The average of each material property across the thickness is kept constant, to ensure that the effect of the through-thickness property variations on the results of the axial and shear load cases would be insignificant.

The first distribution is a symmetric distribution, where the material properties towards the mid-plane of the specimen are greater than the material properties towards the outer surfaces of the specimen. The material parameters are scaled by a factor, SF, where z is the distance from the mid-plane of the specimen. The scaling factor is defined by the function in equation (13). This function is formulated to give an average value of 1. A controls the severity of the variation in properties, while B is the offset value used to control the average value.

$$SF = A \cdot |z| + B \tag{13}$$

The second distribution studied is asymmetrical, where the material properties vary linearly from the one surface to the other. This could possibly occur due to a difference in fibre orientation and fibre volume content across the thickness. The scaling factor for this distribution is defined by the function in equation (14).

$$SF = A \cdot z + B \tag{14}$$

This study is performed for the flexure test, in the 0° directions, with each of the eight layers of elements through the thickness assigned material parameters based on the distributions shown in Fig. 7.

Table 4
Yield function parameters.

k	a	C_{11}	C_{22}	C_{33}	C_{12}	C_{13}	C_{23}	C_{44}	C_{55}	C_{66}
−0.3665	2	1.2179	1.2590	0.9671	0.2961	0.0017	−0.0694	0.86	0.86	0.86

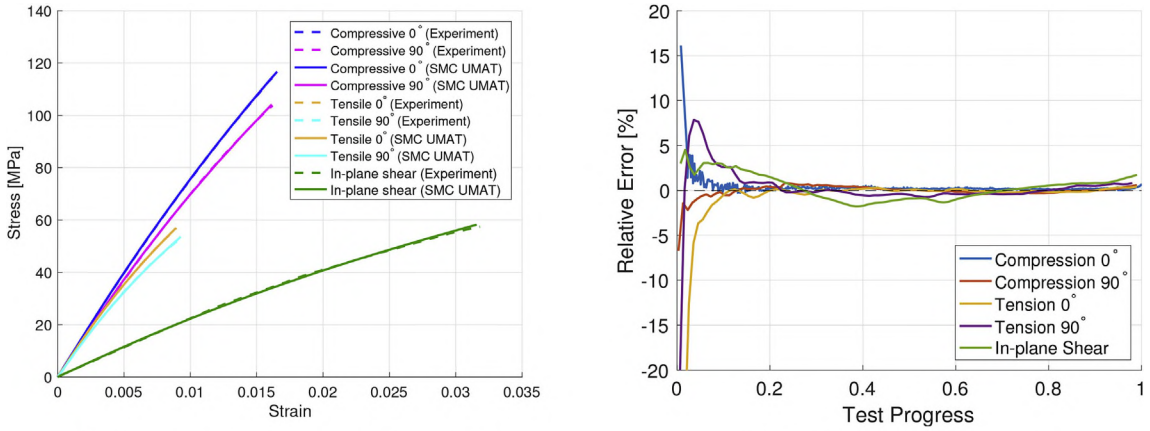

(a) Comparison of stress-strain curves (b) Calibration relative error

Fig. 5. Calibration simulation versus experimental results for tension, compression and in-plane shear tests.

Fig. 8 shows the effect of the variation in through-thickness properties on the flexure response in the 0° direction for the symmetric and asymmetric distributions. In the study of symmetric distributions, the higher the A value, the less stiff the predicted flexure stress-strain response. The decrease in material properties in the outer planes of the specimen had a greater effect than the increase in the material properties in the core of the specimen, resulting in an overall decrease in stiffness in the flexure stress-strain response. This result is expected due to the effects of stiffness on beam bending. In the study of asymmetric distributions the specimen is supported on the less stiff side represented by a positive A value. Increasing A results in a less stiff flexure stress-strain response. This shows that the out-of-plane orientation of specimen can have a significant effect on the result of the experiment if the fibre distribution is not uniform across the thickness.

In order to evaluate the importance of capturing the tension-compression asymmetry of the material when modelling the three-point flexure test, a study is conducted, where the tension-compression asymmetry is removed. The material is assigned properties in the orthotropic axes calibrated using either the tensile test or compressive test data. The results of this study in the 0° and 90° flexure tests are shown in Fig. 9. From the results of the study it is clear that the tension-compression asymmetry has a very significant effect on the flexure response of the material and needs to be considered when modelling such a SMC material. Considering the tension compression asymmetry also has a much larger effect on the results than scaling the through thickness material properties.

Considering only the tensile response causes the model to under

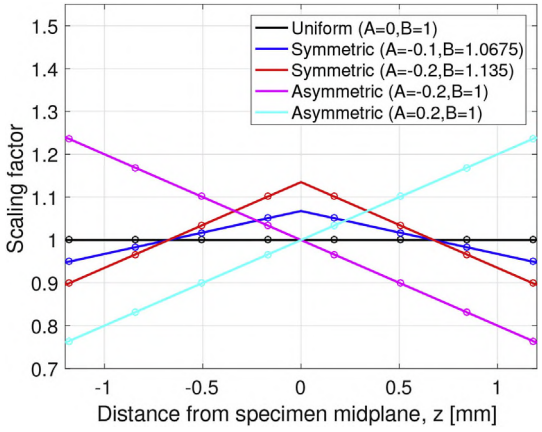

Fig. 7. Scale factor for elastic and hardening parameters for symmetric and asymmetric distributions.

predict the flexure stress strain response. The MAE for the 0° direction increases to 4.9% and in the 90° direction it decreases to 3.0%. Considering only the compressive properties causes the model to over predict the flexure stress strain results with a MAE of 13.7% in the 0° direction and 18.2% in the 90° direction. Therefore, considering the tension compression asymmetry improves the flexure response over only considering the tensile or compressive material properties. The one exception to this is for only considering the tensile properties in the 90°

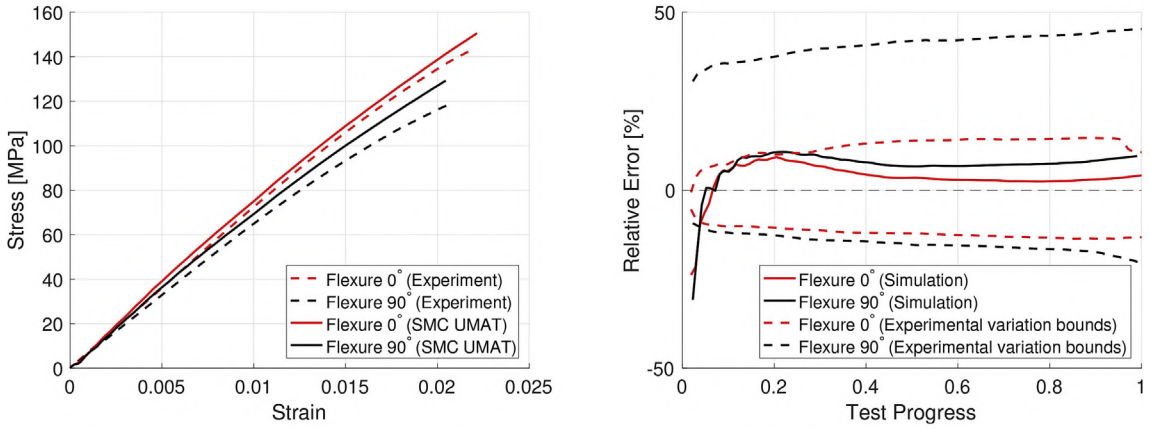

(a) Comparison of stress-strain curves (b) Prediction relative error

Fig. 6. Simulation prediction versus experimental results for flexure tests.

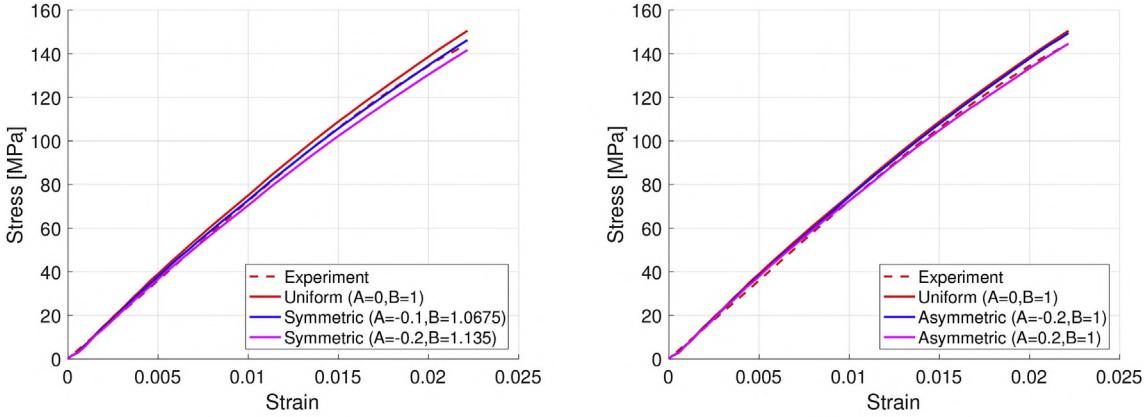

(a) Symmetric (b) Asymmetric

Fig. 8. Parametric study results for various through-thickness property distribution.

direction provides a better prediction, however there is more variation in the experimental results in the 90° direction and considering the tension compression asymmetry falls closer to the middle of the variational bounds than just considering the tensile properties.

6. Conclusion

A SMC material is experimentally investigated in tension, compression, in-plane shear and three-point bending. The material is found to exhibit significant in plane anisotropy as well as tension compression asymmetry in both the elastic and plastic response. To capture this response, an orthotropic elasto-plastic macroscopic phenomenological model is proposed. The model is capable of capturing the tension compression asymmetry in the elastic regime using the stress triaxiality and implements a yield function designed for metals which exhibit similar behaviour coupled with power law hardening to capture the plastic response of the SMC.

The material model is implemented in LS-DYNA as a user-defined

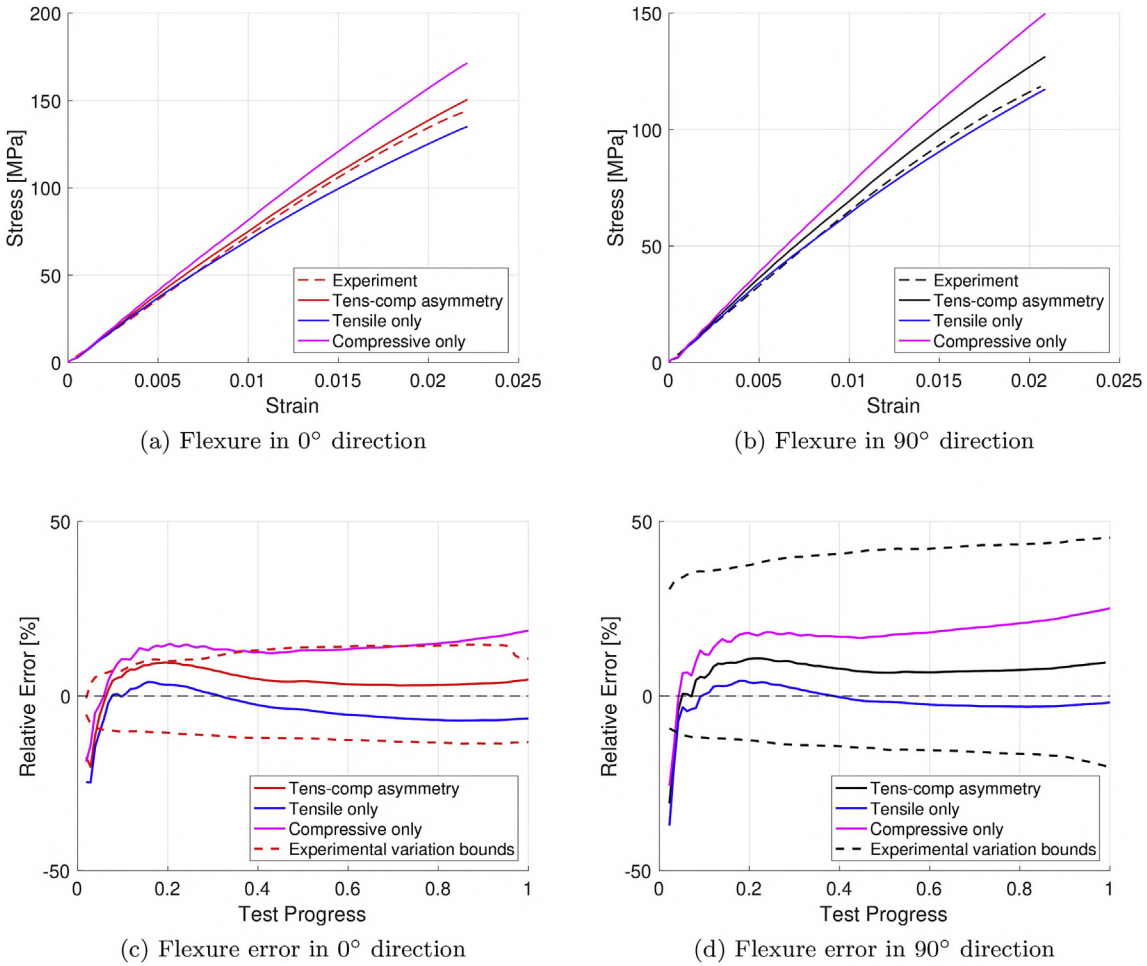

(a) Flexure in 0° direction (b) Flexure in 90° direction

(c) Flexure error in 0° direction (d) Flexure error in 90° direction

Fig. 9. Study of the effect of tension-compression asymmetry on the flexure test.

material model. The material model is calibrated for tensile and compressive tests in the 0° and 90° directions, and the in-plane shear test. The accuracy of the calibration demonstrates the appropriateness of the yield function and hardening rule selected. The calibrated model is able to predict the flexure stress-strain response of the material within 8.1% MAE which is well within the observed experimental variation. However, the model over predicts the average experimental measured stress-strain response. The effects of through thickness variation of material properties and only considering the tensile or compressive properties to simulate the bend test are evaluated. It is found that considering the tension compression asymmetry is necessary to accurately predicting the response of SMC in bending.

Declaration of interest

None.

Acknowledgments

The authors acknowledge Dr. Christopher Kohar for providing code for the yield function. The authors acknowledge the Natural Sciences and Engineering Research Council of Canada (NSERC) PGSD2-489295-2016, the German Research Foundation (DFG) within the International Research Training Group Integrated engineering of continuous-discontinuous long fibre reinforced polymer structures (GRK 2078), and General Motors Corporation for their financial support.

Appendix A. Supplementary data

Supplementary data related to this article can be found at https://doi.org/10.1016/j.compositesb.2018.07.058.

References

[1] NHTSA. National highway traffic safety administration strategic plan 2016-2020. 2016.
[2] Casadei A, Broda R. Impact of vehicle weight reduction on fuel economy for various vehicle architectures. The Aluminum Association, Inc; 2007.
[3] Joost W. Reducing vehicle weight and improving U.S. energy efficiency using integrated computational materials engineering. JOM (J Occup Med) 2012;64:1032–8.
[4] Fuchs E, Field F, Roth R, Kirchain R. Strategic materials selection in the automobile body: economic opportunities for polymer composite design. Compos Sci Technol 2008;68:1989–2002.
[5] Lu K. The future of metals. Science 2010;328:319–20.
[6] Campbell Jr. F. Manufacturing processes for advanced composites. Elsevier; 2003.
[7] Beardmore P, Johnson C. The potential for composites in structural automotive applications. Compos Sci Technol 1986;26:251–81.
[8] Rao NS, Simha T, Rao K, Kumar GR. Carbon composites are becoming competitive and cost effective. Infosys Limited; 2017.
[9] Trauth A, Pinter P, Wedenmenn K. Investigation of quasi-static and dynamic material properties of a structural sheet molding compound combined with acoustic emission damage analysis. Journal of Composite Science 2017:18–36.
[10] Teng T, Ngo V. Analyzing pedestrian head injury to design pedestrian-friendly hoods. Int J Automot Technol 2011;12:213–24.
[11] Ramesh C, Srikari S, Suman M. Design of hood stiffener of a sedan car for pedestrian safety. SASTech, Journal 2012;11:67–73.
[12] Masoumi A, Shojaeefard M, Najibi A. Comparison of steel, aluminum and composite bonnet in terms of pedestrian head impact. Saf Sci 2011;49:1371–80.
[13] Mangino E, Carruthers J, Pitarresi G. The future use of structural composite materials in the automotive industry. Int J Veh Des 2007;44:211–32.
[14] Doghri I, Tinel L. Micromechanics of inelastic composites with misaligned inclusions: numerical treatment of orientation. Comput Meth Appl Mech Eng 2006;195:1387–406.
[15] Lielens G, Pirotte P, Couniot A, Dupret F, Keunings R. Prediction of thermo-mechanical properties for compression moulded composites. Compos Appl Sci Manuf 1998;29:63–70.
[16] Sabiston T, Mohammadi M, Cherkaoui M, Lévesque J, Inal K. Micromechanics for a long fibre reinforced composite model with a functionally graded interphase. Composites Part B 2016;84:188–99.
[17] Sabiston T, Mohammadi M, Cherkaoui M, Lévesque J, Inal K. Micromechanics based elasto-visco-plastic response of long fibre composites using functionally graded interphases at quasi-static and moderate strain rates. Composites Part B 2016;100:31–43.
[18] Carman G, Reifsnider K. Micromechanics of short-fiber composites. Compos Sci Technol 1992;43:137–46.
[19] Panasenko G. Multi-scale modelling for structures and composites. Dordrecht: Springer Netherlands; 2005.
[20] Aboudi J, Arnold S, Bednarcyk B. Micromechanics of composite materials: a generalized multiscale analysis approach. Butterworth-Heinemann; 2012.
[21] LSTC. Material Models LS-DYNA keyword User's manual vol. II. Livermore Software Technology Corporation; 2012.
[22] Huang J, Wang X. Numerical and experimental investigations on the axial crushing response of composite tubes. Compos Struct 2009;91:222–8.
[23] Xiao X, Botkin ME, Johnson NL. Axial crush simulation of braided carbon tubes using mat58 in ls-dyna. Thin-Walled Struct 2009;47:740–9.
[24] Feld N, Maeyens C, Delattre B, Grandmaison N. Modelling the effect of process-induced anisotropy on the constitutive behavior of chopped fiber composites. Compos Appl Sci Manuf 2017;101:334–43.
[25] Oldenbo M, Mattsson D, Varna J, Berglund LA. Global stiffness of a smc panel considering process induced fiber orientation. J Reinforc Plast Compos 2004;23:37–49.
[26] Callister W, Rethwisch D. Materials science and engineering: an introduction. Wiley; 2013.
[27] Donato GHB, Bianchi M. Pressure dependent yield criteria applied for improving design practices and integrity assessments against yielding of engineering polymers. Journal of Materials Research and Technology 2012;1:2–7.
[28] Folgar F, C.T. III. Orientation behavior of fibers in concentrated suspensions. J Reinforc Plast Compos 1984;3:98–119.
[29] Jackson W, Advani S, Tucker C. Predicting the orientation of short fibers in thin compression moldings. J Compos Mater 1986;20:539–57.
[30] Cazacu O, Plunkett B, Barlat F. Orthotropic yield criterion for hexagonal closed packed metals. Int J Plast 2006;22:1171–94.
[31] ASTM D3039/D3039M-17. Standard test method for tensile properties of polymer matrix composite materials. ASTM International; 2017.
[32] ASTM D6641/D6641M-16e1. Standard test method for compressive properties of polymer matrix composite materials using a combined loading compression (CLC) test fixture. ASTM International; 2016.
[33] ASTM D5379/D5379M-12. Standard test method for shear properties of composite materials by the V-Notched beam method. ASTM International; 2012.
[34] Lee S, Munro M. Evaluation of in-plane shear test methods for advanced composite materials by the decision analysis technique. Composites 1986;17:13–22.
[35] Plastics. Determination of flexural properties (ISO/DIS 178:2017). ISO; 2017.
[36] Lempriere B. Poisson's ratio in orthotropic materials. AIAA J 1968;6:2226–7.
[37] Ludwik P. Elemente der Technologischen Mechanik. Springer-Verlag Berlin Heidelberg; 1909.
[38] Williams B, Simha C, Abedrabbo N, Mayer R, Worswick M. Effect of anisotropy, kinematic hardening, and strain-rate sensitivity on the predicted axial crush response of hydroformed aluminium alloy tubes. Int J Impact Eng 2010;37:652–61.
[39] Kohar C, Mohammadi M, Mishra R, Inal K. The effects of the yield surface curvature and anisotropy constants on the axial crush response of circular crush tubes. Thin-Walled Struct 2016;106:28–50.
[40] Yoon J, Barlat F, Dick R, Chung K, Kang T. Plane stress yield function for aluminum alloy sheetspart II: FE formulation and its implementation. Int J Plast 2004;20:495–522.
[41] Abedrabbo N, Pourboghrat F, Carsley J. Forming of AA5182-O and AA5754-O at elevated temperatures using coupled thermo-mechanical finite element models. Int J Plast 2007;23:841–75.
[42] Willmott C, Matsuura K. Advantages of the mean absolute error (MAE) over the root mean square error (RMSE) in assessing average model performance. Clim Res 2005;30:79–82.
[43] Chen Z, Huang T, Shao Y, Li Y, Xu H, Avery K, Zeng D, Chen W, Su X. Multiscale finite element modeling of sheet molding compound (SMC) composite structure based on stochastic mesostructure reconstruction. Compos Struct 2018;188:25–38.
[44] Matzenmiller A, Lubliner J, Taylor R. A constitutive model for anisotropic damage in fiber-composites. Mech Mater 1995;20:125–52.
[45] Ryou H, Chung K, Yu W-R. Constitutive modeling of woven composites considering asymmetric/anisotropic, rate dependent, and nonlinear behavior. Composites Part A 2007;38:2500–10.